

SCALING-UP DEEP LEARNING PREDICTIONS OF HYDROGRAPHY FROM IFSAR DATA IN ALASKA

L. V. Stanislawski^{1*}, E. J. Shavers¹, A. J. Duffy², P. Thiem¹, N. Jaroenchai³, S. Wang³, Z. Jiang⁴, B. J. Kronenfeld⁵, B. P. Buttenfield⁶

¹ U.S. Geological Survey, Center of Excellence for Geospatial Information Science, 1400 Independence Road, Rolla Missouri, 65401, United States (lstan, eshavers, pthiem)@usgs.gov,

² University of Missouri Science & Technology, Rolla Missouri, United States aduffy@contractor.usgs.gov,

³ Department of Geography and Geographic Information Science, University of Illinois at Urbana-Champaign, United States (nj7, shaowen)@illinois.edu,

⁴ Computer & Information Science & Engineering, University of Florida, United States zhe.jiang@ufl.edu,

⁵ Department of Geology and Geography, Eastern Illinois University, United States bjchronenfeld@eiu.edu,

⁶ Department of Geography, University of Colorado-Boulder, United States babs@colorado.edu

ISPRS WG IV/4, III/10, IV/7, V/1 & ICWG IV/III - Free and Open Source Software for Geospatial (FOSS4G) 2022

KEY WORDS: elevation, hydrography, machine learning, U-net, transfer learning, National Hydrography Dataset.

ABSTRACT:

The United States National Hydrography Dataset (NHD) is a database of vector features representing the surface water features for the country. The NHD was originally compiled from hydrographic content on U.S. Geological Survey topographic maps but is being updated with higher quality feature representations through flow-routing techniques that derive hydrography from high-resolution elevation data. However, deriving hydrography through flow-routing methods is a complex process that needs to be tailored to different geographic conditions, which can lead to varying solutions. To address this problem, this paper evaluates automated deep learning and its transferability to extract hydrography from interferometric synthetic aperture radar (IfSAR) elevation data spanning a range of geographic conditions in Alaska.

1. INTRODUCTION

The U.S Geological Survey (USGS) has been providing topographic maps and geospatial data for the United States for over 125 years (USGS, National Geospatial Program, 2022). Serving as a primary access point for freely available geospatial data and topographic maps, The National Map is a suite of products and services for viewing and downloading base topographic information to support science investigations, emergency operations, and numerous other activities. In a new initiative to deliver higher-quality data and support improved geospatial analysis, the USGS is upgrading the elevation and hydrography datasets into the 3D National Topography Model (3DNTM), which will include fully integrated hydrography and elevation. The USGS 3D Elevation Program (3DEP) recently completed acquisition of interferometric synthetic aperture radar (IfSAR) elevation data at 5-meter spatial resolution for Alaska (USGS, 2022). Other parts of the United States are being mapped at higher resolution with lidar-derived elevation data. This paper describes a research effort by the USGS that applies machine learning methods to extract hydrographic features from IfSAR data in Alaska to improve the National Map hydrographic database.

Under the 3DNTM, new hydrography data are acquired through methods that derive or extract the features directly from high-resolution 3DEP elevation data to ensure proper integration of the hydrography and elevation layers. By applying specifications for deriving 1:24,000 or larger scale hydrography from high resolution elevation data (Archuleta and Terziotti, 2020; Terziotti and Archuleta, 2020), a tenfold increase in the number of features in the National Hydrography Dataset (NHD) is expected (Anderson, Rea, Lucas, 2021). Consequently, highly

automated machine learning methods to extract and validate the hydrography data collection are being investigated to meet this production challenge.

Deep learning methods to extract hydrography from light detection and ranging (lidar) and other remotely sensed data have shown promising results in recent years (Bernhardt et al., 2020; Chen et al., 2018; Chen et al., 2020; Wang et al., 2020; Xu et al., 2019; Xu et al., 2021). Xu et al. (2021) demonstrated that the U-net (Ronneberger, Fischer, and Brox, 2015) fully convolutional neural network (CNN) is capable of extracting hydrography from lidar elevation data with 80 to 90 percent accuracy. Stanislawski et al. (2021) applied a U-net model using several IfSAR and IfSAR-derived input layers to predict hydrography for a 50-watershed study area in north-central Alaska, where average F1-score accuracies of 68 percent were achieved on test watersheds. Subsequently, the U-net model for predicting hydrography from IfSAR in Alaska was improved by enhancing the reference training data and the input data layers, which yielded average F1-scores of better than 80 percent for the test watersheds (Stanislawski et al., 2022).

Transfer learning approaches are being tested through this research to expand or scale-up implementation of the U-net model to extract hydrography for other areas of Alaska. Transfer learning methods apply feature relations (in the form of weights from a trained model) learned from one domain and apply them to another domain, which can greatly reduce training requirements for the new domain (Kimura et al., 2020). For example, a transfer learning process achieved 94 percent accuracy in predicting the quality of roads in Nigeria based on a model originally trained to predict road quality in the United States (Brewer et al., 2021). In our application, a *base* model

trained in one geographic area is transferred to another geographic *target* area to reduce training requirements for the target area. Preliminary research by Jaroenchai and Wang (2022) demonstrated transfer learning to predict stream hydrography features from lidar-derived input layers. The base CNN models achieved F1-scores of about 82 percent for a watershed in North Carolina and the transfer-learned model achieved F1-scores of about 70 percent for a target watershed in Virginia, which was 5 to 6 percent better and required much less training than the trained-from-scratch models for the target area. Research presented in this paper builds upon that work by testing transfer learning methods to scale-up hydrography predictions from IfSAR in Alaska. The base model for this study is an improved version of the U-net model developed by Stanislawski et al. (2021).

The following sections describe methods and preliminary results on development of a U-net model to predict hydrography from IfSAR data in a 50-watershed study area in Alaska, which serves as a base model. In addition, transfer learning methods are described to apply the base model to an adjacent 74-watershed target area. The effect of distance from training data on the quality of transfer learning solutions is measured to help quantify training data requirements.

2. METHODS

2.1 Study Area and Data

The study area and geographic domain for the base CNN model covers more than 4600 square kilometers (km²) in north-central Alaska and includes fifty 12-digit Hydrologic Unit (HU12) watersheds (west study area in Figures 1 and 2). In the geographic domain of the base model, elevation ranges from 32 m to 1911 m above sea level (Figure 2, west area). The southern half of the base model domain includes a section of the Kobuk River valley with a broad low relief flood plain area with wetlands, meandering channels, and many ponds. Relief rises abruptly north of the Kobuk River valley into the Endicott Mountains where elevation rises above 1900 m. The larger lakes in this study area, Avaraart and Kolliksak Lakes, are each less than 3 km².

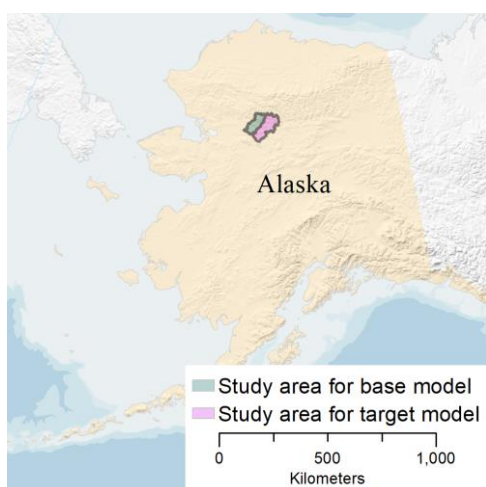


Figure 1. Location of areas in Alaska for base neural network model and target transfer learning model.

The target study area, where transfer learning methods are tested, covers more than 7400 km² and includes 74 HU12 watersheds that are just east of the base study area (Figures 1

and 2). Elevation ranges from 64 to 2460 m above sea level in the target study area. The geographic domain covers the eastern part of the Kobuk River watershed from the headwaters in the Endicott Mountains in the northern half of the study area to the lower relief Kobuk River valley in the middle to southern portions of the area, which also includes the Pah River valley. The six larger lakes in the target study area range in size from about 3 km² for Lake Minakokosa up to about 38 km² for Walker Lake. Additional larger lakes listed in increasing size include Narvak Lake, Lake Selby, Walker Lake, and Norutak Lake. Thus, a notable difference between the base and target study areas is that the target study area includes several lakes that are much larger than the largest lakes in the study area used to train the base model.

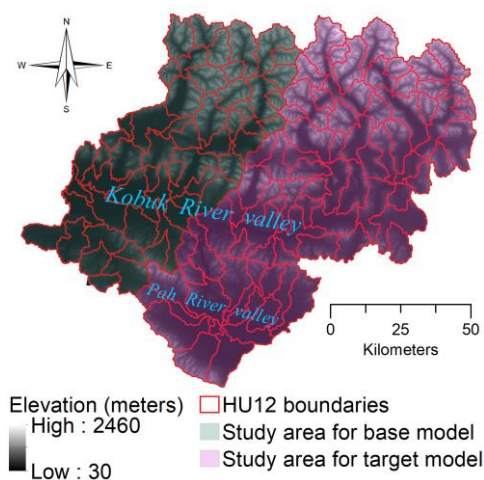


Figure 2. Elevation and 12-digit hydrologic unit (HU12) boundaries for base and target model areas.

2.1.1 IfSAR Data: IfSAR-derived digital terrain model (DTM), digital surface model (DSM), and orthorectified radar intensity (ORI) datasets that are freely downloadable from the USGS are used in this study (USGS, 2017a, 2017b, and 2017c). The IfSAR data were collected between August 2012 and August 2013 using P- and X-band radar frequencies optimized for terrain conditions ranging from glacial surfaces, bare or vegetated surfaces, to dense tree canopies (Kampes et al., 2011). The DTM provides a 5-m resolution model estimated from the bare earth elevation radar returns. In contrast, the DSM provides a 5-m resolution surface model determined from radar elevation returns from all features, including vegetation and buildings. A root mean square error of elevation returns estimated for the radar data collected in this project ranges from about 0.55 m to 1.54 m (Stanislawski et al., 2021). USGS contractors are required to hydro-flatten large waterbody features greater than 8000 square meters in the IfSAR elevation products. These large waterbodies, which are identified through radar response characteristics and visual inspection, are flattened to the elevation of the lowest bounding cell. The ORI for the study areas are 0.625-m resolution radar backscatter intensity images.

2.1.2 Reference Hydrography: The reference hydrography (Figure 3) is vector-based NHD features that were originally compiled by USGS contractors to 1:24,000-scale (24k) specifications (Archuleta and Terziotti, 2020; Terziotti and Archuleta, 2020). The 24k hydrography was derived from the IfSAR DTM and ORI data using proprietary workflows of contractors that vertically and horizontally align the features

with the channels in the DTM and hydrographic breaklines (i.e., hydro-flattened waterbodies) in the ORI data. Panchromatic and color-infrared Statewide Ortho Image satellite data at 1.5-m and 2.5-m resolution were provided by Alaska GeoNorth Information Systems to guide visual editing and validation of the reference features. The vector reference features are vertically and horizontally aligned with the elevation data and form a complementary dataset to the elevation for testing hydrography feature extraction from the IfSAR data. Reference data are used to train CNN models and test the accuracy of the model predictions for both the base and target study areas.

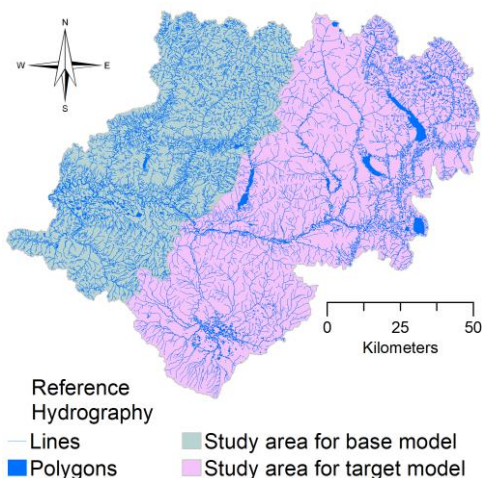


Figure 3. Reference 1:24,000-scale hydrographic features derived from IfSAR data through contracted work for the U.S. Geological Survey.

2.2 Base Model

The U-net model is applied in this study for both base and target area models. U-net is a fully CNN that uses an encoder-decoder architecture with a contractive and expanding path (Ronneberger, Fischer, and Brox, 2015). U-net applies multiple convolutional and max pooling layers in the contractive path to extract global general feature information. In the expanding path, U-net applies several convolutional layers to extract detailed localized information, which is concatenated with the global information to generate pixel-wise feature predictions through a sigmoid activation function. Each convolution is batch normalized (Ioffe and Szegedy, 2015) with a batch size of 16 and applies a rectified linear unit (Relu) activation function to identify and preserve important characteristics and reduce redundancy and noise. Additional details of the model architecture are described in Stanislawski et al. (2021). Figure 4 displays the reference features and HU12 boundaries for the training and test watersheds within the base model domain. For training, 4000 56x56-pixel window patches are used from each of the 10 training watersheds, which includes 1600 selected patches and 2400 patches derived from augmentation per watershed. For each training watershed, the 1600 selected sample patches are distributed over 160 square grids (10 patches per grid) that subdivide the watershed, with 800 patches centered on water features and 800 centered on non-water features. Then 400 patches of the 1600 samples (i.e., 1/4th) are randomly selected for six augmentation operations, which include two rotations, two scalings, one shear, and one mirror. Thus, 40,000 56x56 patches are used for training the base model with one-third of the sample patches used for training and two

thirds used for testing. Training minimizes the loss function, which is the negative Dice coefficient (Dice, 1945), and continues for a maximum of 50 epochs with a learning rate of 0.0001.

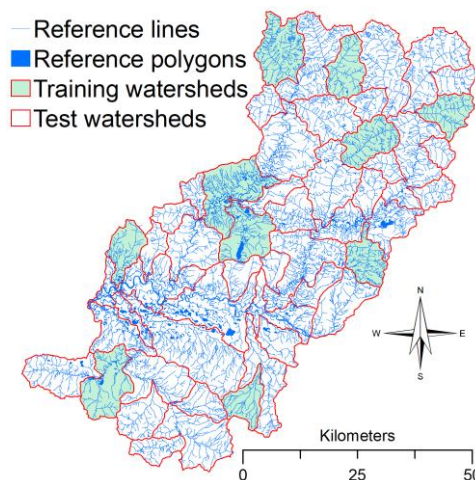


Figure 4. Reference 1:24,000-scale hydrographic features with training and testing watersheds for the base model study area.

2.2.1 Input Layers: Overall, 16 data layers related to surface hydrology are generated, coordinated with identical raster projection systems, and used as input for the U-net models. All layers are resampled to 5-m resolution and co-registered in the Albers Equal Area projection for Alaska using the North American Datum of 1983. Layers include DEM, DSM, ORI, non-linear filtered DTM (Perona and Malik, 1990), curvature (Sangireddy et al., 2016), geomorphons (Jasiewicz and Stepinski, 2013), a 2-D shallow-water channel depth (SWCD) model with a highly diffusive surface (Mitasova, et al., 2004), topographic wetness index (Moore, Grayson, and Ladson, 1991), negative openness (Doneus, 2013), positive openness (Doneus, 2013), sky view factor (Zakšek, Oštir, and Kokalj, 2011), sky illumination (Kennelly and Stewart, 2014), topographic position index based on a 3x3-pixel window (Deumlich, Schmidt, and Sommer, 2010), topographic position index based on an 11x11-pixel window, 2-D SWCD with default diffusion, and a one-hot 2-D SWCD default diffusion layer. The one-hot raster includes only ones (true) and zeros (false).

The first 14 of these layers are the same layers included in models tested by Stanislawski et al. (2021), which provided average F1-scores of 68 percent for test watersheds. The last two layers are associated with the default diffusion SWCD model and are included in these new models because it was determined that the SWCD is substantially more influential to model predictions than the next most important layer (Stanislawski et al., 2021). Therefore, we refined the SWCD model parameters to apply the default diffusion and roughness values. A threshold value that identifies likely inundated pixels in channels and waterbodies is determined for each watershed, and pixels with SWCD value greater than the threshold are included in the binary one-hot 2-D SWCD layer.

The threshold SWCD value is determined from the histogram of the SWCD values for a watershed as the first value after the

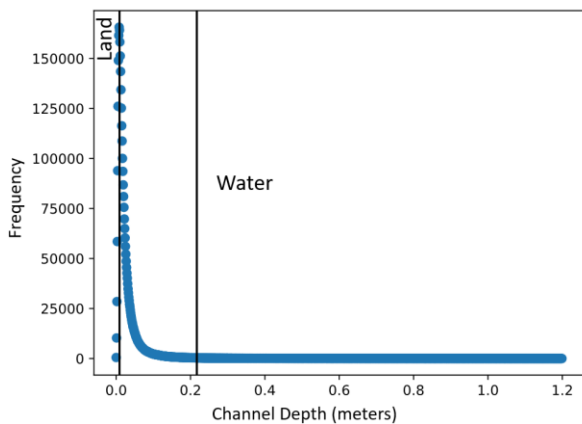


Figure 5. Histogram of 2-D shallow water channel depth values for a watershed with mode threshold of likely land (non-water) and second derivative threshold for likely water.

mode where the second derivative of the histogram is nearly zero (i.e., less than 0.01). An example histogram of SWCD values with the mode and second derivative threshold is shown in Figure 5.

A workflow was developed to automate downloads and processing of IfSAR-derived tiles of DTM, DSM, and ORI data for user-selected watersheds from the 3DEP database (<https://code.usgs.gov/cegis-hydronet/upscale-ak-hydronet>). The workflow mosaics common tiles and derives the raster data layers from the DTM that are related to surface hydrology and used as input layers for the U-net models. The data processing workflows are implemented with Python, Linux shell scripts, and opensource software libraries such as the Geospatial Data Abstraction Library (GDAL).

2.2.2 Raster Reference Layers: A separate 5-m resolution reference raster dataset representing water and non-water pixels is generated for each HU12 watershed from the vector hydrography reference data. The reference raster is co-registered with all input layers. Elevation-derived hydrography specifications indicate that single-line streams can range up to 30 m in width (Terziotti and Archuleta, 2020). Therefore, the SWCD model is used to estimate channel width of the reference flow network line features. The reference network lines are rasterized with a variable-sized buffer by excluding pixels from a 20-m buffer around the line features that are not within the associated one-hot SWCD layer. Any pixels within a 2.5-m buffer around the network features that were excluded through the variable-buffer process are re-added into the reference raster dataset to retain connectivity as represented in the vector version of the reference flow network. Subsequently, pixels within a raster version of the reference hydrography polygons are included in the rasterized reference network pixels to form the Boolean reference raster dataset for a watershed.

The traditional flow-routing and other geomorphometric techniques used to collect the vector reference hydrography from the IfSAR are sensitive to terrain and vegetation conditions and workflow parameterizations, which may produce variable results. In fact, the reference hydrography for this study represents initial efforts to derive hydrography from IfSAR data, and therefore the quality of the reference data is likely inadequate in places. Consequently, a masked reference layer is generated to filter likely errors in the reference data, and it is

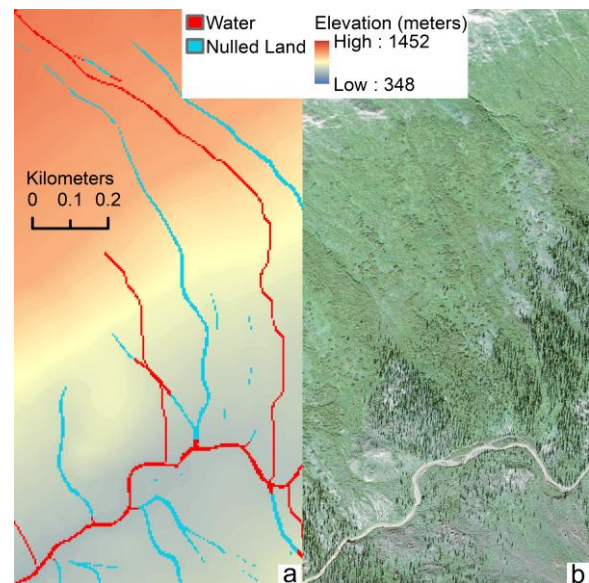


Figure 6. (a) Section of a masked reference dataset with nulled water values that are excluded from accuracy assessment, and (b) Maxar 0.5-m resolution satellite image data of the same area.

used to form a supplementary, more optimistic estimate for model prediction accuracy. This masked reference dataset consists of the reference raster dataset excluding land (non-water) pixels that are likely water and water pixels that are likely land (Figure 6). Land pixels that are likely water are found in slope-derived depression areas and/or areas with pixels having SWCD values that are larger than the second derivative threshold (Figure 5). Water pixels that are likely land are pixels with SWCD values that are smaller than the mode threshold (Figure 5). Excluded pixels are not counted in the masked accuracy tests.

2.3 Transfer Learning

Knowledge from the base U-net model that was trained on the base model study area is transferred to a U-net model for the target 74-HU12 study area. Deep neural network models applied to natural image datasets tend to learn standard or general features in the first layer for different datasets, training objectives and cost functions, and features learned in the last layer are specific to the dataset and task (Shirokikh et al., 2020; Yosinski et al., 2014). For this study, we transfer the base model to the target area by first importing the base models' weights and freezing the last two layers (classifier part) while training the model with the training samples from the target area using a standard 0.0001 learning rate. The general knowledge in the weights should enable the model to train quickly with less training data. After the general feature training, all layers are unfrozen and retrained with a substantially reduced learning rate (0.000001) to refine the model to the target domain.

Training levels for the transfer learning models are chosen to assess whether model prediction accuracy decreases with distance from training areas. Eight levels of training are tested for the transfer learning models: four use 1000 56x56-pixel sample patches per watershed, and the second four use 4000 56x56-pixel patches per watershed. Model 1 uses only one watershed for training, which is labelled number 1 in Figure 7. Model 2 uses the two watersheds for training that are labelled 1 and 2 in Figure 7. Likewise, models 3 and 4 respectively use the

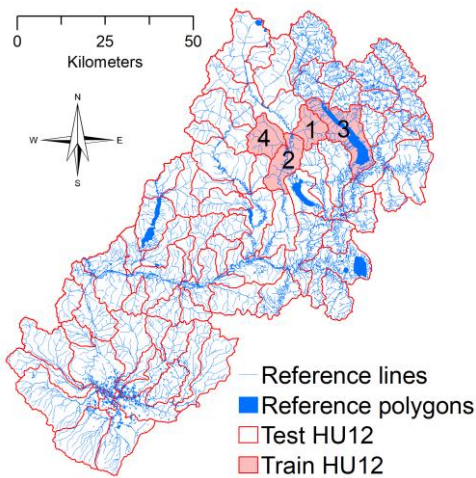


Figure 7. Vector reference hydrography with the four training watersheds numbered for the target study area domain.

first three and four labelled watersheds in Figure 7 for training. Thus, two versions of the four models are trained: one version using 1000 patches per watershed, and the second version with 4000 patches per watershed. The 56x56-pixel sample patches are selected, distributed, augmented, and implemented with the same proportions as applied for the base model sample design.

2.4 Training from Scratch

In training from scratch, the U-net model is trained using the same reference and input data layers as used for the transfer learning models. However, no weights are transferred from the base model, and no layers are frozen. Each model is trained from scratch using the same sample window patches and augmentations that were used for the transfer learning tests. All eight levels of training that were used for transfer learning tests are also used for the training from scratch tests to provide direct comparisons with the transfer learning results.

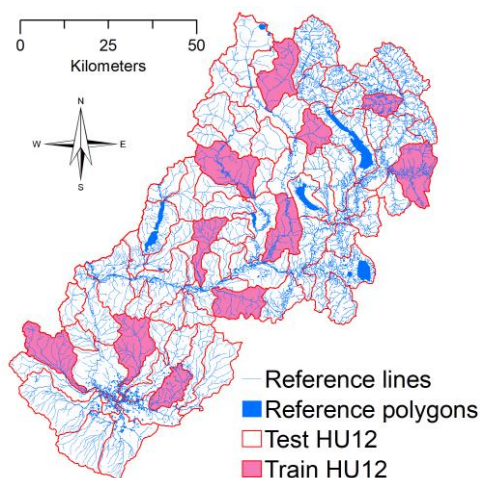


Figure 8. Distribution of 11 training watersheds in the target study area that are used for a best training from scratch model.

In addition, a U-net model is trained on the target study area with the same level of training that was used for the base model. Eleven of the 74 watersheds in the study area are used for training this model (Figure 8), each with 4000 56x56-pixel sample patches of which 1600 are evenly distributed over water and non-water areas and the remaining 2400 patches are generated from augmentations as was done for the base model. The eleven training watersheds represent about 15 percent of the target study area and are distributed over the study area as was done for the base model (Figure 8). This model should provide a reasonable estimate of a best possible training from scratch model with prediction results that are similar to the base model.

2.5 Model Accuracy Tests

For each model, test watersheds are the non-trained watersheds. Precision, recall, and F1-scores are averaged for all training watersheds and for all test watersheds for each level of training. To determine if the distance from training data affects transfer learning accuracy, the distance between the centroid of each test watershed and the centroid of the training watershed is determined, and the F1-scores of test watersheds are plotted against distance from training centroid.

Neural network modelling is implemented through TensorFlow and Keras (<https://code.usgs.gov/aduffy/geoflow/-/tree/singleres>), and data processing is completed on a 12-node Linux cluster or through GPU nodes on the USGS Tallgrass computing facilities (<https://hpcportal.cr.usgs.gov/hpc-user-docs/Tallgrass/Overview.html>).

3. PRELIMINARY RESULTS AND DISCUSSION

F1-scores shown in Figure 9 summarize accuracy results for the base model. F1-scores for the training watersheds range from 64 to 89 percent and average 77 percent. F1-scores for training watersheds determined from the filtered (masked) reference data range from 68 to 95 percent and average 83 percent. For the test watersheds, unfiltered F1-scores range from 52 to 90 percent and average 72 percent, and masked F1-scores range from 57 to 95 percent and average 78 percent. Accuracy only diminishes about 5 percent on average between the training and test watersheds, indicating that the model is well trained and provides stable results for the base model study area.

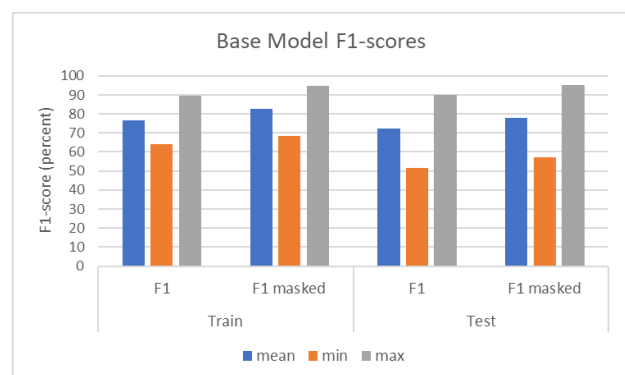


Figure 9. F1-scores for the base model study area summarized for training and test watersheds based on unfiltered and filtered (masked) reference data.

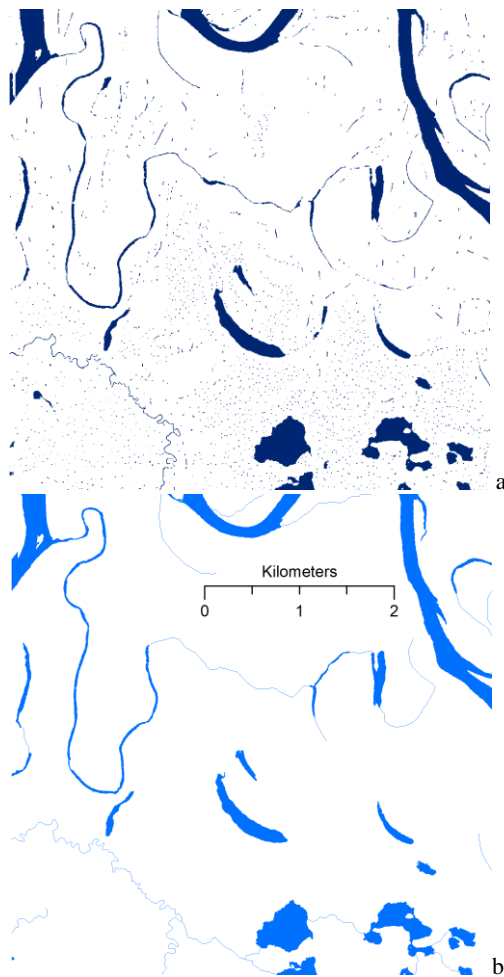


Figure 10. Example of typical hydrography predictions from the base model (a), and the reference vector hydrography (b).

An example of typical raster-based hydrography predicted for a section of the base model study area is shown in Figure 10, along with the associated reference hydrography. Model predictions are quite accurate for large waterbodies and wider stream features. The predictions show many small waterbodies or depressions in the flood plain area. Specifications for the collected reference data (Archuleta and Terziotti, 2020) prohibits collection of lake/pond features that are less than 30 m along the shortest axis or less than 0.4 hectare (about 160 5-m pixels). The precision, or level of detail of the reference waterbody features limits both the ability to assess the quality of predictions and to train models to find small waterbody features. Filtering small clumps of predicted water pixels can eliminate much of these over-extracted features, but it can also eliminate sections of thin drainage channels that are not well connected. It is also noted from Figure 10 that some network features are not predicted or are not well connected, particularly in the low relief flood plain area with many small pond-like depressions. Low relief areas with many depressions, wetlands and small drainage channels are typical conditions where the U-net models fail to provide adequate predictions. Further research would be useful to address these problem areas.

Transfer learning accuracy results will be summarized at the conference, along with a comparative assessment with the base model and training from scratch predictions. The level at which transfer learning prediction accuracy deteriorates with distance from training data will be a key characteristic limiting the

usability of this approach. The further transfer learning solutions can be accurately implemented without additional training data the more cost effective the solutions will be.

4. CONCLUDING REMARKS

Mapping hydrography for the state of Alaska is a daunting task, given its vast area and terrain that is difficult to navigate. Big challenges with large high-quality datasets are well suited to take advantage of recent advancements in neural networks (Usery et al., 2021). This research demonstrates the tremendous potential to improve and speed up mapping of surface water features in Alaska, and elsewhere in the world having challenging terrain and limited resources.

Reported accuracy scores measure how well a machine can reproduce hydrography generated with meticulous editing by numerous subject matter experts. It is not a score of how well the surface water features are mapped by the model. The human factor in contemporary broad scale mapping efforts cannot be ignored and warrants consideration as a source of uncertainty in the related accuracy metrics. How well the maps fit what is on the ground can only be definitively confirmed by being on the ground at any given point in time, as hydrologic conditions are constantly in flux. Thus, the work here could be used as an aid to human cartographers in their efforts to interpret what is important to the map user.

This work could also benefit change detection efforts. As new and better elevation data are collected, automated strategies such as the model presented here could be used to identify regions with significant changes in surface water distribution. This type of automation would be valuable to maintain an accurate national map over time and help address the numerous challenges that society faces related to hydrology.

DISCLAIMER

Any use of trade, firm, or product names is for descriptive purposes only and does not imply endorsement by the U.S. Government.

REFERENCES

- Anderson, R., Rea, A., and Lucas, V., 2021., The next generation of hydrography. U.S. Geological Survey, August 25, 2021. <https://www.usgs.gov/media/videos/next-generation-hydrography> (Accessed July 7, 2022).
- Archuleta, C.M., and Terziotti, S., 2020. Elevation-derived hydrography—representation, extraction, attribution, and delineation rules. U.S. Geological Survey Techniques and Methods 11-B12: Reston, VA, USA. <https://pubs.er.usgs.gov/publication/tm11B12>.
- Bernhardt, H., Garcia, D., Hagensieker, R., Mateo-Garcia, G., Lopez-Francos, I., Stock, J., Schumann, G., Dobbs, K., Kalaitzis, F. 2020. Waters of the United States: Mapping America's waters in near real-time. In Earth Science, Artificial Intelligence 2020: Ad Astra per Algorithmos; Frontier Development Lab, National Aeronautics and Space Administration; SETI Institute: Mountain View, CA, USA, pp. 243–269.

- Brewer, E., Lin, J., Kemper, P., Hennin, J., Runfola, D. 2021. Predicting road quality using high resolution satellite imagery: A transfer learning approach. *PLoS ONE* 16(7): e0253370. <https://doi.org/10.1371/journal.pone.0253370>
- Chen, Y., Fan, R., Yang, X., Wang, J., Latif, A. 2018. Extraction of urban water bodies from high-resolution remote-sensing imagery using deep learning. *Water* 2018, 10, 585.
- Chen, Y., Tang, L., Kan, Z., Bilal, M., Li, Q. 2020. A novel water body extraction neural network (WBE-NN) for optical high-resolution multispectral imagery. *J. Hydrol.* 2020, 588, 125092.
- Deumlich, D., Schmidt, R., Sommer, M. 2010. A multiscale soil–landform relationship in the glacial-drift area based on digital terrain analysis and soil attributes. *J. Plant Nutr. Soil Sci.*, 173, 843–851.
- Dice, L.R. 1945. Measures of the amount of ecologic association between species. *Ecology*, 26, 297–302.
- Doneus, M. 2013. Openness as visualization technique for interpretative mapping of airborne lidar derived digital terrain models. *Remote Sens.*, 5, 6427–6442.
- Ioffe, S. Szegedy, C. 2015. Batch normalization: Accelerating Deep network training by reducing internal covariate shift. In *Proceedings of the 32nd International Conference on Machine Learning*, Lille, France. *J. Mach. Learn. Res.* 2015, 37, 9.
- Jaroenchai, N., and Wang, S. 2022. Transfer learning with convolutional neural networks for hydrological streamline detection. *American Association of Geographers Annual Meeting*, February 26-March 1, 2022.
- Jasiewicz, J., Stepinski, T. 2013. Geomorphons—A pattern recognition approach to classification and mapping of landforms. *Geomorphology*, 182, 147–156.
- Kampes, B.; Blaskovich, M.; Reis, J.J.; Sanford, M.; Morgan, K. 2011. Fugro GEOSar airborne dual-band IFSAR DTM processing. In *Proceedings of the ASPRS 2011 Annual Conference*, Milwaukee, WI, USA, 1–5 May 2011.
- Kennelly, P.J., Stewart, A.J. 2014. General sky models for illuminating terrains. *Int. J. Geogr. Inf. Sci.*, 28, 383–406.
- Kimura, N., Yoshinaga, I., Sekijima, K., Azechi, I., and Baba, D. 2020. Convolutional neural network coupled with a transfer-learning approach for time-series flood predictions. *Water*, 12, 96. <https://doi.org/10.3390/w12010096>
- Mitasova, H., Thaxton, C., Hofierka, J., McLaughlin, R., Moore, A., Mitas, L. 2004. Path sampling method for modeling overland water flow, sediment transport, and short-term terrain evolution in Open Source GIS. *Dev. Water Sci.*, 55, 1479–1490.
- Moore, I.D., Grayson, R.B., Ladson, A.R. 1991. Digital terrain modeling: A review of hydrological, geomorphological, and biological applications. *Hydrol. Process.*, 5, 3–30.
- Perona, P. Malik, J. 1990. Scale-space and edge detection using anisotropic diffusion. *IEEE Trans. Pattern Anal. Mach. Intell.*, 12, 629–639.
- Ronneberger, O., Fischer, P., and Brox, T., 2015. U-net: Convolutional networks for biomedical image segmentation. In *International Conference on Medical Image Computing and Computer-Assisted Intervention*; Springer: Cham, Switzerland; New York, NY, USA.
- Sangireddy, H., Stark, C.P., Kladzyk, A., Passalacqua, P. 2016. GeoNet: An open source software for the automatic and objective extraction of channel heads, channel network, and channel morphology from high resolution topography data. *Environ. Model. Softw.*, 83, 58–73.
- Shirokikh, B., Zakazov, I., Chernyavskiy, A., Fedulova, I., and Belyaev, M. 2020. First U-net layers contain more domain specific information than the last ones. In: et al. *Domain Adaptation and Representation Transfer, and Distributed and Collaborative Learning*. DART 2020, DCL 2020. *Lecture Notes in Computer Science*, vol 12444. Springer, Cham. https://doi.org/10.1007/978-3-030-60548-3_12
- Stanislawski, L.V., Shavers, E.J., Duffy, A., Thiem, P., Kronenfeld, B.J., and Buttenfield, B.P., 2022. Assessment of vector hydrography derived from deep learning of remotely sensed data. *American Association of Geographers Annual Meeting*, February 26-March 1, 2022.
- Stanislawski, L.V., Shavers, E.J., Wang, S., Jiang, Z., Usery, E.L., Moak, E., Duffy, A., and Schott, J., 2021. Extensibility of U-Net neural network model for hydrographic feature extraction and implications for hydrologic modeling. *Remote Sensing* 13, no. 12: 2368. <https://doi.org/10.3390/rs13122368>.
- Terziotti, S., and Archuleta, C.M., 2020. Elevation-derived hydrography acquisition specifications. *U.S. Geological Survey Techniques and Methods 11-B11*: Reston, VA, USA, <https://doi.org/10.3133/tm11B11>.
- USGS, National Geospatial Program, 2022. History: 125 years of topographic mapping. U.S. Geological Survey, <https://www.usgs.gov/programs/national-geospatial-program/history-1>. (Accessed May 24, 2022).
- USGS. 2022. Alaska Mapping Initiative. <https://www.usgs.gov/ngp-user-engagement-office/alaska-mapping-initiative>. (Accessed May 24, 2022).
- U.S. Geological Survey. 2017a. 5 Meter Alaska digital elevation models (DEMs) - USGS National Map 3DEP downloadable data collection. U.S. Geological Survey, <https://www.sciencebase.gov/catalog/item/5641fe98e4b0831b7d62e758> (Accessed on 10 March 2022).
- U.S. Geological Survey. 2017b. Alaska digital surface models (DSMs) - USGS National Map 3DEP downloadable data collection. <https://www.sciencebase.gov/catalog/item/543e6a6ae4b0fd76af69cf47> (accessed on 10 May 2021).
- U.S. Geological Survey. 2017c. Alaska orthorectified radar intensity image - USGS National Map 3DEP downloadable data collection. <https://www.sciencebase.gov/catalog/item/543e6acde4b0fd76af69cf4a> (accessed on 10 May 2021).

Usery, E.L., Arundel, S.T., Shavers, E., Stanislawski, L., Thiem, P. and Varanka, D., 2021. GeoAI in the US Geological Survey for topographic mapping. *Transactions in GIS*, 26(1), 25-40.

Wang, G., Wu, M., Wei, X., Song, H. 2020. Water identification from high-resolution remote sensing images based on multidimensional densely connected convolutional neural networks. *Remote Sens.* 2020, 12, 795.

Xu, Z., Jiang, Z., Shavers, E.J., Stanislawski, L.V., Wang, S. 2019. A 3D convolutional neural network method for surface water mapping using lidar and NAIP imagery. In *Proceedings of the ASPRS-International Lidar Mapping Forum*, Denver, CO, USA, 25–31 January 2019.

Xu, Z., Wang, S., Stanislawski, L.V., Jiang, Z., Jaroenchai, N., Sainju, A.M., Shavers, E., Usery, E.L., and Chen, L., 2021. An attention U-Net model for detection of fine-scale hydrologic streamlines. *Env. Model. Softw.* 140, 104992. <http://doi.org/10.1016/j.envsoft.2021.104992>.

Yosinski, J., Clune, J., Bengio, Y., and Lipson, H. 2014. How transferable are features in deep neural networks? In: *Advances in Neural Information Processing Systems*. pp. 3320-3328.

Zakšek, K., Oštir, K., Kokalj, Ž. 2011. Sky-view factor as a relief visualization technique. *Remote Sens.*, 3, 398–415.